Atomic electron tomography in three and four dimensions

Jihan Zhou[1], Yongsoo Yang[2], Peter Ercius[3], Jianwei Miao[1]*

1. Department of Physics & Astronomy and California NanoSystems Institute, University of California, Los Angeles, CA 90095, USA.

2. Department of Physics, Korea Advanced Institute of Science and Technology (KAIST), Daejeon 34141, South Korea.

3. National Center for Electron Microscopy, Molecular Foundry, Lawrence Berkeley National Laboratory, Berkeley, CA 94720, USA.

Atomic electron tomography (AET) has become an increasingly important tool for atomic scale structural characterization in three and four dimensions. It provides the ability to correlate structures and properties of materials at the single atomic level. With recent advances in data acquisition methods, iterative 3D reconstruction algorithms, and post-processing methods, AET can now determine the 3D atomic coordinates and chemical species with sub-Angstrom precision, and further reveal their atomic scale time evolution during dynamical processes. Herein, we summarize the recent progress in developing AET through selected highlights of recent findings on the determination of 3D coordinates in materials and capturing how the atoms rearrange during early nucleation at 4D atomic resolution.

Keywords: Atomic electron tomography (AET), transmission electron microscopy (TEM), scanning transmission electron microscopy (STEM), and 4D atomic resolution.

I. Introduction

Recent years have witnessed an increasing demand of developing novel nanomaterials and nanostructures for applications in catalysis,[1-5] electronics,[6-8] energy conversion and storage,[9-11] quantum materials,[12-14] high performance metals,[15-17] biosensing and target delivery.[18-20] To custom and tailor their

functional properties, it is prerequisite to determine their 3D atomic structures including crystal defects and disorders, such as grain boundaries, dislocations, interfaces and point defects. Furthermore, optimizing material synthesis and fabrication is essential in designing devices with desired properties, and to achieve this, determination of the 3D structure is not enough. It is required to measure their atomic-scale dynamics during the sample fabrication process and under working condition of the device.

Transmission electron microscopy is routinely capable of imaging atomic structures, but only provides 2D projection views of 3D crystalline samples. Scanning probe microscopy can image surface structures at atomic resolution, but is blind to sub-surface structures. Among several powerful 3D imaging and structural determination methods including crystallography,[21-22] coherent diffractive imaging,[23-25] cryo-electron microscopy,[26-28] and atom probe tomography,[29-30] electron tomography has proven to be an important tool to image the 3D structure of heterogeneous biological and physical samples with nanometer resolution.[31-33] By using crystallinity and other prior knowledge as constraints, electron tomography has been applied to image the 3D structure of various nanostructures with atomic resolution from a single or few projection images.[34-40] However, because of making a few assumptions, this is not a general method to determine the 3D crystal defects and disordered structures. This major obstacle was overcome by the demonstration of AET in 2012, enabling to achieve 2.4 Å resolution without assuming crystallinity for the first time.[41] In 2015, AET was further advanced to determine the 3D coordinates of individual atoms in materials with a precision of 19 picometer.[42] The transformation from electron tomography at nanometer resolution[43-52] to AET capable of identifying 3D atomic positions in materials represents a quantum leap from qualitative to quantitative material characterization. Subsequently, AET has been applied to study crystal defects such as grain boundaries, dislocations, stacking faults, point defects and strain tensors with unprecedented 3D detail.[41-42,53-56] The experimental atomic coordinates have also been used as direct input to *ab initio* calculations to

correlate 3D atomic structures and the physical, chemical and electronic properties of materials at the single-atom level.[55]

In this article, we review the experimental and computational aspects of AET, including data acquisition, image denoising and alignment, 3D image reconstruction, atom tracing, classification and refinement. We illustrate recent developments in determining the 3D atomic coordinates and chemical order/disorder of nanomaterials. We also highlight the first experimental observation of early nucleation dynamics with 4D AET (i.e. space + time).[56] Finally, we discuss the future challenges and opportunities of this powerful method for material characterization in the 21st century.

II. From pictures to 3D atomic coordinates: quantitative electron microscopy in 3D and 4D

II.1 Acquisition of tomographic tilt series

Electron tomography reconstructs 3D structural information from a tilt series of 2D electron microscopy images usually acquired at many different viewing angles.[33,57-60] The resolution of an electron tomography reconstruction is set by the tilt range, the number of tilt angles, the dose applied to the sample, and the resolution of 2D projected images. Enormous efforts have been employed to improve the resolution limit and stability of electron microscopy since its invention,[61-63] and aberration corrected electron microscopy can now routinely achieve sub-Angstrom resolution with much-improved image contrast.[64] Although AET was first demonstrated on conventional electron microscopy,[41,54] aberration corrected electron microscopy has significantly facilitated the data acquisition for AET. To reduce the diffraction contrast and the multiple scattering effects, annular dark field (ADF)-STEM has usually been used to acquire tomographic tilt series. As the sample damage is the main issue in data acquisition, the following approaches have been implemented to mitigate the radiation damage, including (i) choosing appropriate operating voltages; (ii) deposition of a thin protective layer (e.g. carbon film) over the specimen; (iii) finding the maximum tolerable electron dose for a specific sample; (iv) reducing the unnecessary dose on a sample as

much as possible; (v) taking multiple images at each angle and then aligning them to improve the signal-to-noise ratio.

II.2 Image pre-processing

Before the AET reconstruction, proper image post-processing must be done to remove any undesired effects such as image distortion due to drift, scan coil distortion, and noise. The multiple images (typically 3 – 10) acquired at each tilt angle are used to estimate and correct the specimen drift.[42,55-56,65] The scanning coil related distortions are corrected by applying a non-linear, microscope-specific correction matrix obtained by analyzing a reference specimen with known lattice parameters.[42,55-56,66] The signal to noise ratio of each image is further improved by applying advanced denoising techniques.[67] Next, each tilt series is aligned to a common tilt axis using two approaches. Parallel to the tilt axis direction, the images are aligned to each other with sub-pixel accuracy by the common-line method.[68,69] Perpendicular to the tilt axis direction, the alignment is achieved by the center of mass (CoM) method.[41-42,54-56] The CoM of each image is located and the image is shifted so that the CoM coincides with the origin. This procedure is repeated until all the images are aligned. These methods have been successful for achieving high-accuracy alignment of electron tomography tilt series.[41-42,54-56]

II.3 Advanced iterative reconstruction algorithms

AET tilt series has two intrinsic issues: i) the missing wedge problem (i.e. the tilt range beyond ±75° cannot usually be measured),[58] and ii) a limited number projection images due to the radiation damage.[70] Conventional tomographic methods such as filtered (or weighted) back projection[33,71] cannot produce good quality reconstructions due to the incomplete data. Over the years, several iterative algorithms have been developed to alleviate this incomplete data problem.[72-74] One method, termed GENeralized Fourier Iterative REconstruction (GENFIRE), has recently proven to be effective in reconstructing 3D atomic structure from a limited number projects with a missing wedge.[55,56,75,76] GENFIRE first assembles a 3D reciprocal grid from the experimental 2D projections using oversampled to increase the gridding accuracy. The algorithm

then iterates on the 3D grid between real and reciprocal space to search for a global solution that is consistent with the measured data (reciprocal space) and general physical constraints such as positivity and support (real space). The GENFIRE algorithm is described in **Figure 1**a.

II.4 Post-processing of reconstructions: Atom tracing, species classification, and refinement

The 3D atomic positions and species can be determined from the reconstruction. Figure 1b shows a cross-sectional view of a typical AET reconstruction of an FePt nanoparticle. The positions of local maxima within the volume represent the positions of each atom in the nanoparticle. By applying a local maxima tracing algorithm, the 3D atomic coordinates can be precisely determined.[42,55-56] Atoms with larger atomic number (Z) will show higher intensities than those of lower Z elements for ADF-STEM tomography. The chemical species of each traced atom is classified based on the relative intensity contrast between different chemical species known to exist in a sample. Figure 1b shows that there are local maxima with relatively stronger intensity (Pt atoms) and weaker intensity (Fe atoms). Figure 1c shows the histogram of 5 × 5 × 5 voxels integrated intensities from the reconstruction volume for all traced atoms. Two Gaussian-shaped peaks are observed with some overlap. Most of the atoms can be clearly classified as Fe or Pt atoms based on their intensity. However, there are some ambiguous atoms at the overlapping region which need to be further classified. To separate these ambiguous atoms, an unbiased atom classification method can be used.[55] By comparing the volume profile of every traced atom with the averaged volume profile of each chemical species, all atoms can be iteratively re-classified until a self-consistent average volume profile is reached. This method provides consistent classification results regardless of the initial starting configuration.[55,56] The obtained 3D atomic model (both atomic coordinates and chemical species) can be further refined by minimizing the error between the measured and simulated projections along the experimental tilt angles.[42,55-56]

III. Advances in atomic electron tomography

III.1 3D atomic imaging of nanostructures

3D atomic imaging of complex nanostructures with crystal defects such as grain boundaries, stacking faults, dislocations and chemical distribution has been demonstrated with the acquisition of an atomically resolved tilt series and subsequent tomographic reconstruction. By combining ADF-STEM and an iterative reconstruction algorithm called equal slope tomography (EST), Scott et al. have first demonstrated that AET can image a gold nanoparticle at 2.4 Å resolution without assuming crystallinity.[41] **Figure 2**a shows four major crystal grains, and individual atoms are observed in some regions in the nanoparticle. A similar approach was applied to study dislocations in a platinum nanoparticle. Chen et al. enhanced the signal-to-noise ratio of the reconstruction using 3D Fourier filtering.[54] Figure 2b shows a 5.3 Å thick internal slice of the nanoparticle. A zigzag pattern, the characteristic feature of a screw dislocation core are visible in the enlarged views.

Haberfehlner et al. demonstrated atomic resolution electron tomography on silver/gold core/shell nanoclusters using fewer numbers of projections and the SIRT reconstruction algorithm.[77] From the reconstruction obtained by thirty-one STEM projections taken between 72^{o} and -70^{o}, the 3D morphology and composition of a cluster containing gold- and silver-rich regions can be identified without using any prior information and with minimal filtering (Figure 2c). By searching for confined maxima, they found the atomic positions localized within the cluster volume. This 3D information provides insight on the growth and deposition process of the nanocluster.

Using the *ab initio* single-nanoparticle reconstruction method, Park et al. for the first time determined the 3D structures of platinum nanocrystals in graphene liquid cells at near atomic resolution.[78] Figure 2d shows the 3D reconstruction of a Pt nanoparticle and the cross-sectional view along the vertical plane with tentative atomic positions indicated. This experiment provides means to understand the structure and stability of nanocrystals in liquid.

III.2 Pinpointing atom locations and chemical order in three dimensions

The first demonstration of precise (±19 pm precision) 3D atomic structural determination of thousands of individual atoms via AET was reported in 2015 by Xu et al.[42] They measured the full atomic coordinates of 3769 atoms which form the first nine atomic layers of a tungsten needle tip sample (**Figure 3**a). Furthermore, the atomic displacement field and the full 3D strain tensor was calculated with a resolution of 1 nm^3 and a precision of 10^{-3}, respectively. Density functional theory calculations and molecular dynamics simulations verified that the observed strain originates from the tungsten carbide formed at the surface of the tip and diffusion of carbon several layers inside the needle.

Another important breakthrough has been made for measuring the chemical order/disorder atomic structure of transition metal based alloy compounds. Yang et al. applied AET to precisely determine the 3D coordinates (±22pm precision) and chemical species (99% accuracy) of an FePt nanoparticle.[55] The internal chemically ordered grain structure was fully characterized. A rich structural variety of grain boundaries, anti-phase boundaries, anti-site point defects and swap defects were observed (Figure 3b-c). The experimentally measured coordinates and chemical species were directly input to DFT calculations. The spin and orbital magnetic moments were successfully determined for individual atoms within an $L1_0$ phase grain, showing variations depending on local atomic coordinates and chemical ordering. Furthermore, local magnetocrystalline anisotropy (MAE), the main property of interest for magnetic device applications, can also be calculated, which showed direct correlation with the local order parameters (Figure 3d). This work demonstrates not only the capabilities of AET to precisely determine full 3D atomic coordinates and chemical species of complex nanomaterials but also AET can be combined with quantum mechanical calculations to reveal the physical properties at the atomic scale. This paves a new way to advance our understanding of structure-property relationships of functional materials.

III.3 Capturing atom motion in 4D

While the 3D static atomic structure of materials is important to understand their functionality, there exists significant interest to reveal the

structure and dynamics of materials at 4D atomic resolution to study processes such as nucleation and growth. Using FePt nanoparticles as a model system, Zhou et al. have recently studied the dynamics of of early stage nuclei in an *ex-situ* AET experiment (**Figure 4**).[56] Selected FePt nanoparticles were first annealed at 520 °C in vacuum for 9 min, and tilt series were measured of each at room temperature. Then the nanoparticles were further annealed (520 °C) and measured at room temperature for 2-3 different annealing times. For all measured tilt series, 3D atomic models were obtained and analyzed using the same reconstruction method. Figure 4a shows the atomic models of the same nanoparticle with an accumulated annealing time of 9 min, 16 min and 26 min, respectively. The atoms on and near the surface rearrange to form $L1_0$ phases while the Pt-rich core of the nanoparticle stays nearly the same (Figure 4b) which is evident when comparing the same internal atomic layers along the [010] direction (Figure 4c). By tracking the common nuclei in the particle, they found that early-stage nuclei are irregularly shaped, each has a core of one to a few atoms with the maximum order parameter, and the initiation of nucleation mainly occurs on the surface of the nanoparticles. The nuclei can undergo growth (Figure 4d), fluctuation (Figure 4e-g), dissolution(Figure 4h), merging and/or division (Figure 4f-g), depending on the order parameter gradient distribution as well as thermodynamics and kinetics. These results not only show a never-before-seen view of nucleation but also indicate that a theory beyond classical nucleation theory is needed to describe early-stage nucleation at the atomic scale. This experiment adds a new dimension (time) to AET (i.e. 4D AET), capturing atomic motion in materials in four dimensions, which is currently not accessible by any other experimental methods. 4D AET will potentially serve as a powerful tool in studying many fundamental problems such as phase transitions, atomic diffusion, grain boundary dynamics, interface motion, defect dynamics and surface reconstruction.

IV. Summary and outlook

With the recent development of electron microscopy, data analysis procedure, advanced iterative reconstruction algorithms, atom tracing and refinement methods, AET has made several breakthroughs. Now, we are in the era of

precisely determining the 3D positions of individual atoms in materials and probing their dynamics at 4D atomic resolution. Several examples of AET in 3D and 4D were summarized in this review. The future research frontiers of AET bring up more challenges and opportunities in solving fundamental problems such as disorder structures, electron beam sensitive structures and *in situ* 3D atomic dynamics. Several novel techniques could be employed to further improve the capabilities of AET, such as ptychography,[79-81] atomic elemental mapping,[82-83] 4D-STEM,[84-85] dose-efficient STEM,[86] low-dose modality imaging schemes with either advanced direct electron detectors[87] or cryogen temperature environment,[88-89] and *in situ* atomic imaging microscopy.[90-91] On the algorithm and method side, new method,[92] new reconstruction algorithm[93] and machine learning could further extend the applicability of AET to 2D materials, heterostructures, thin films and other material systems. With a combination of novel imaging modes and advanced reconstruction algorithms, we anticipate AET will play a key part in solving many fundamental problems in materials science, nanoscience, condensed matter physics and chemistry.

Acknowledgments

This work was supported by STROBE, A National Science Foundation Science & Technology Center (DMR-1548924), the Office of Basic Energy Sciences of the US DOE (DE-SC0010378), an Army Research Office MURI grant on Ab-Initio Solid-State Quantum Materials: Design, Production and Characterization at the Atomic Scale (18057522), and the Division of Materials Research of the US NSF (DMR-1437263). P. E. is supported by the Molecular Foundry, Lawrence Berkeley National Laboratory, which is supported by the U.S. Department of Energy under contract no. DE-AC02-05CH11231. Y. Y. acknowledges the support by the National Research Foundation of Korea (NRF) grant funded by the Korea government (MEST) (No. 2019R1F1A1058236), and the KAIST-funded Global Singularity Research Program (M3I3).

References

1. V.R. Stamenkovic, B. Fowler, B.S. Mun, G. Wang, P.N. Ross, C.A. Lucas and N.M. Marković, *Science* **315**, 493 (2007).

2. Y. Ding and M. Chen, *MRS Bull.* **34**, 569 (2009).

3. B. Lim, M. Jiang, P.H.C. Camargo, E.C. Cho, J. Tao, X. Lu, Y. Zhu and Y. Xia, *Science* **324**, 1302 (2009).

4. X. Huang, Z. Zhao, L. Cao, Y. Chen, E. Zhu, Z. Lin, M. Li, A. Yan, A. Zettl, Y.M. Wang, X. Duan, T. Mueller and Y. Huang, *Science* **348**, 1230 (2015).

5. L. Lin, W. Zhou, R. Gao, S. Yao, X. Zhang, W. Xu, S. Zheng, Z. Jiang, Q. Yu, Y.-W. Li, C. Shi, X.-D. Wen and D. Ma, *Nature* **544**, 80 (2017).

6. M. Law, J. Goldberger and P. Yang, *Annu. Rev. Mater. Res.* **34**, 83 (2004).

7. B. Tian, X. Zheng, T.J. Kempa, Y. Fang, N. Yu, G. Yu, J. Huang and C.M. Lieber, *Nature* **449**, 885 (2007).

8. L. Dou, A.B. Wong, Y. Yu, M. Lai, N. Kornienko, S.W. Eaton, A. Fu, C.G. Bischak, J. Ma, T. Ding, N.S. Ginsberg, L.-W. Wang, A.P. Alivisatos and P. Yang, *Science* **349**, 1518 (2015).

9. A.S. Aricò, P. Bruce, B. Scrosati, J.-M. Tarascon and W. van Schalkwijk, *Nat. Mater.* **4**, 366 (2005).

10. B. Kang and G. Ceder, *Nature* **458**, 190 (2009).

11. H. Sun, J. Zhu, D. Baumann, L. Peng, Y. Xu, I. Shakir, Y. Huang and X. Duan, *Nat. Rev. Mater.* **4**, 45 (2019).

12. X. Qian, J. Liu, L. Fu and J. Li, *Science* **346**, 1344 (2014).

13. P. Liu, J.R. Williams and J.J. Cha, *Nat. Rev. Mater.* **4**, 479 (2019).

14. X. Liu and M.C. Hersam, *Nat. Rev. Mater.* **4**, 669 (2019).

15. Y. Wang, M. Chen, F. Zhou and E. Ma, *Nature* **419**, 912 (2002).

16. B. Gludovatz, A. Hohenwarter, D. Catoor, E.H. Chang, E.P. George and R.O. Ritchie, *Science* **345**, 1153 (2014).

17. E. Lilleodden and P. Voorhees, *MRS Bull.* **43**, 20 (2018).

18. N.L. Rosi and C.A. Mirkin, *Chem. Rev.* **105**, 1547 (2005).

19. P.D. Howes, R. Chandrawati and M.M. Stevens, *Science* **346**, 1247390 (2014).

20. Y. Ding, Z. Jiang, K. Saha, C.S. Kim, S.T. Kim, R.F. Landis and V.M. Rotello, *Mol. Ther.* **22**, 1075 (2014).

21. M. Ladd, R. Palmer, *Structure determination by X-ray crystallography*, (Plenum Press, NewYork, US, 1994).

22. J. Drenth, *Principles of Protein X-ray Crystallography* (Springer, New York, US, 1994).

23. J. Miao, P. Charalambous, J. Kirz, D. Sayre, *Nature* **400**, 342 (1999).

24. I. Robinson, R. Harder, *Nat. Mater.* **8**, 291 (2009).

25. J. Miao, T. Ishikawa, I. K. Robinson, M. M. Murnane, *Science* **348**, 530 (2015).

26. Y. Cheng, *Cell* **161**, 450 (2015).

27. E. Nogales, *Nat. Methods* **13**, 24–27 (2016).

28. P. Zhang, *Curr. Opin. Struct. Biol.* **58**, 249 (2019).

29. T. F. Kelly, M. K. Miller, *Rev. Sci. Instrum.* 78, 031101 (2007).

30. D. Seidman and K. Stiller, *MRS Bull.* **34**, 717 (2009).

31. D. J. de Rosier , A. Klug , *Nature* **217**, 130 (1968).

32. R. G. Hart, *Science* **159**, 1464 (1968).

33. J. Frank, *Electron Tomography: Methods for Three-Dimensional Visualization of Structures in the Cell* (Springer, 2010).

34. Z.Y. Li, N.P. Young, M. Di Vece, S. Palomba, R.E. Palmer, A.L. Bleloch, B.C. Curley, R.L. Johnston, J. Jiang and J. Yuan, *Nature* **451**, 46 (2008).

35. S. Van Aert, K.J. Batenburg, M.D. Rossell, R. Erni and G. Van Tendeloo, *Nature* **470**, 374 (2011).

36. B. Goris, S. Bals, W. Van den Broek, E. Carbó-Argibay, S. Gómez-Graña, L.M. Liz-Marzán and G. Van Tendeloo, *Nat. Mater.* **11**, 930 (2012).

37. D. Van Dyck, J.R. Jinschek and F.-R. Chen, *Nature* **486**, 243 (2012).

38. J. Hwang, J.Y. Zhang, A.J. D'Alfonso, L.J. Allen and S. Stemmer, *Phys. Rev. Lett.* **111**, 266101 (2013).

39. M. Azubel, J. Koivisto, S. Malola, D. Bushnell, G.L. Hura, A.L. Koh, H. Tsunoyama, T. Tsukuda, M. Pettersson, H. Häkkinen and R.D. Kornberg, *Science* **345**, 909 (2014).

40. C.L. Jia, S.B. Mi, J. Barthel, D.W. Wang, R.E. Dunin-Borkowski, K.W. Urban and A. Thust, *Nat. Mater.* **13**, 1044 (2014).

41. M.C. Scott, C.-C. Chen, M. Mecklenburg, C. Zhu, R. Xu, P. Ercius, U. Dahmen, B.C. Regan and J. Miao, *Nature* **483**, 444 (2012).

42. R. Xu, C.-C. Chen, L. Wu, M.C. Scott, W. Theis, C. Ophus, M. Bartels, Y. Yang, H. Ramezani-Dakhel, M.R. Sawaya, H. Heinz, L.D. Marks, P. Ercius and J. Miao, *Nat. Mater.* **14**, 1099 (2015).

43. P.A. Midgley and M. Weyland, *Ultramicroscopy* **96**, 413 (2003).

44. P.A. Midgley, J.M. Thomas, L. Laffont, M. Weyland, R. Raja, B.F.G. Johnson and T. Khimyak, *J. Phys. Chem. B* **108**, 4590 (2004).

45. I. Arslan, T.J.V. Yates, N.D. Browning and P.A. Midgley, *Science* **309**, 2195 (2005).

46. P. Ercius, M. Weyland, D.A. Muller and L.M. Gignac, *Appl. Phys. Lett.* **88**, 243116 (2006).

47. S. Bals, K.J. Batenburg, J. Verbeeck, J. Sijbers and G. Van Tendeloo, *Nano Lett.* **7**, 3669 (2007).

48. E.P.W. Ward, T.J.V. Yates, J.-J. Fernández, D.E.W. Vaughan and P.A. Midgley, *J. Phys. Chem. C* **111**, 11501 (2007).

49. T. Yaguchi, M. Konno, T. Kamino and M. Watanabe, *Ultramicroscopy* **108**, 1603 (2008).

50. H.L. Xin, P. Ercius, K.J. Hughes, J.R. Engstrom and D.A. Muller, *Appl. Phys. Lett.* **96**, 223108 (2010).

51. A. Genc, L. Kovarik, M. Gu, H. Cheng, P. Plachinda, L. Pullan, B. Freitag and C. Wang, *Ultramicroscopy* **131**, 24 (2013).

52. J. Zhou, M. Taylor, G.A. Melinte, A.J. Shahani, C.C. Dharmawardhana, H. Heinz, P.W. Voorhees, J.H. Perepezko, K. Bustillo, P. Ercius and J. Miao, *Sci. Rep.* **8**, 10239 (2018).

53. J. Miao, P. Ercius and S.J.L. Billinge, *Science* **353**, aaf2157 (2016).

54. C.-C. Chen, C. Zhu, E.R. White, C.-Y. Chiu, M.C. Scott, B.C. Regan, L.D. Marks, Y. Huang and J. Miao, *Nature* **496**, 74 (2013).

55. Y. Yang, C.-C. Chen, M.C. Scott, C. Ophus, R. Xu, A. Pryor, L. Wu, F. Sun, W. Theis, J. Zhou, M. Eisenbach, P.R.C. Kent, R.F. Sabirianov, H. Zeng, P. Ercius and J. Miao, *Nature* **542**, 75 (2017).

56. J. Zhou, Y. Yang, Y. Yang, D.S. Kim, A. Yuan, X. Tian, C. Ophus, F. Sun, A.K. Schmid, M. Nathanson, H. Heinz, Q. An, H. Zeng, P. Ercius and J. Miao, *Nature* **570**, 500 (2019).

57. P.A. Midgley, E.P.W. Ward, A.B. Hungría and J.M. Thomas, *Chem. Soc. Rev.* **36**, 1477 (2007).

58. P.A. Midgley and R.E. Dunin-Borkowski, *Nat. Mate.* **8**, 271 (2009).

59. Z. Saghi and P.A. Midgley, *Annu. Rev. Mater. Res.* **42**, 59 (2012).

60. P. Ercius, O. Alaidi, M.J. Rames and G. Ren, *Adv. Mater.* **27**, 5638 (2015).

61. M. Haider, S. Uhlemann, E. Schwan, H. Rose, B. Kabius and K. Urban, *Nature* **392**, 768 (1998).

62. P. E. Batson, N. Dellby, O. L. Krivanek, *Nature* **418**, 617 (2002).

63. S.J. Pennycook, *Ultramicroscopy* **180**, 22 (2017).

64. R. Erni, M.D. Rossell, C. Kisielowski and U. Dahmen, *Phys. Rev. Lett.* **102**, 096101 (2009).

65. C. Ophus, J. Ciston and C.T. Nelson, *Ultramicroscopy* **162**, 1 (2016).

66. K. G. Larkin, M. A. Oldfield, H. Klemm, *Opt. Commun*. **139**, 99 (1997).

67. K. Dabov, A. Foi, V. Katkovnik, K. Egiazarian, *IEEE Trans. Image Process.* **16**, 2080–2095 (2007).

68. R. A. Crowther, L. A. Amos, J. T. Finch, D. J. De Rosier, A. Klug, *Nature*. **226**, 421–425 (1970).

69. Y. Liu, P. A. Penczek, B. F. McEwen, J. Frank, *Ultramicroscopy*. **58**, 393 (1995).

70. R. F. Egerton, P. Li, M. Malac, *Micron*. **35**, 399 (2004).

71. J. Frank, *Three-Dimensional Electron Microscopy of Macromolecular Assemblies* (Oxford University Press, 2006).

72. R. Gordon, R. Bender, G. T. Herman, *J. Theor. Biol.* **29**, 471 (1970).

73. A. H. Andersen, A. C. Kak, *Ultrason. Imaging*. **6**, 81 (1984).

74. J. Miao, F. Förster, O. Levi, *Phys. Rev. B.* **72**, 052103 (2005).

75. A. Pryor, Y. Yang, A. Rana, M. Gallagher-Jones, J. Zhou, Y. H. Lo, G. Melinte, W. Chiu, J. A. Rodriguez, J. Miao, *Sci. Rep.* **7**, 10409 (2017).

76. Y. H. Lo, C.-T. Liao, J. Zhou, A. Rana, C. S. Bevis, G. Gui, B. Enders, K. M. Cannon, Y.-S. Yu, R. Celestre, K. Nowrouzi, D. Shapiro, H. Kapteyn, R. Falcone, C. Bennett, M. Murnane, J. Miao, *Sci. Adv.* **5**, eaax3009 (2019).

77. G. Haberfehlner, P. Thaler, D. Knez, A. Volk, F. Hofer, W.E. Ernst and G. Kothleitner, *Nat. Commun.* **6**, 8779 (2015).

78. J. Park, H. Elmlund, P. Ercius, J.M. Yuk, D.T. Limmer, Q. Chen, K. Kim, S.H. Han, D.A. Weitz, A. Zettl and A.P. Alivisatos, *Science* **349**, 290 (2015).

79. H. Yang, R.N. Rutte, L. Jones, M. Simson, R. Sagawa, H. Ryll, M. Huth, T.J. Pennycook, M.L.H. Green, H. Soltau, Y. Kondo, B.G. Davis and P.D. Nellist, *Nat. Commun.* **7**, 12532 (2016).

80. S. Gao, P. Wang, F. Zhang, G.T. Martinez, P.D. Nellist, X. Pan and A.I. Kirkland, *Nat. Commun.* **8**, 163 (2017).

81. Y. Jiang, Z. Chen, Y. Han, P. Deb, H. Gao, S. Xie, P. Purohit, M. W. Tate, J. Park, S. M. Gruner, V. Elser, D. A. Muller, *Nature*. **559**, 343 (2018).

82. D.A. Muller, L.F. Kourkoutis, M. Murfitt, J.H. Song, H.Y. Hwang, J. Silcox, N. Dellby and O.L. Krivanek, *Science* **319**, 1073 (2008).

83. Q. Ding, Y. Zhang, X. Chen, X. Fu, D. Chen, S. Chen, L. Gu, F. Wei, H. Bei, Y. Gao, M. Wen, J. Li, Z. Zhang, T. Zhu, R.O. Ritchie and Q. Yu, *Nature* **574**, 223 (2019).

84. H. Yang, L. Jones, H. Ryll, M. Simson, H. Soltau, Y. Kondo, R. Sagawa, H. Banba, I. MacLaren, P. D. Nellist, *J. Phys. Conf. Ser.* **644**, 012032 (2015).

85. W. Gao, C. Addiego, H. Wang, X. Yan, Y. Hou, D. Ji, C. Heikes, Y. Zhang, L. Li, H. Huyan, T. Blum, T. Aoki, Y. Nie, D. Schlom, R. Wu and X. Pan, *Nature* (2019). doi:10.1038/s41586-019-1649-6.

86. C. Ophus, J. Ciston, J. Pierce, T.R. Harvey, J. Chess, B.J. McMorran, C. Czarnik, H.H. Rose and P. Ercius, *Nat. Commun.* **7**, 10719 (2016).

87. D. Zhang, Y. Zhu, L. Liu, X. Ying, C.-E. Hsiung, R. Sougrat, K. Li and Y. Han, *Science* **359**, 675 (2018).

88. Y. Li, Y. Li, A. Pei, K. Yan, Y. Sun, C.-L. Wu, L.-M. Joubert, R. Chin, A.L. Koh, Y. Yu, J. Perrino, B. Butz, S. Chu and Y. Cui, *Science* **358**, 506 (2017).

89. M.J. Zachman, Z. Tu, S. Choudhury, L.A. Archer and L.F. Kourkoutis, *Nature* **560**, 345 (2018).

90. H. Yoshida, Y. Kuwauchi, J.R. Jinschek, K. Sun, S. Tanaka, M. Kohyama, S. Shimada, M. Haruta and S. Takeda, *Science* **335**, 317 (2012).

91. H.-G. Liao, L. Cui, S. Whitelam and H. Zheng, *Science* **336**, 1011 (2012).

92. X. Tian, D. S. Kim, S. Yang, C. J. Ciccarino, Y. Gong, Yo. Yang, Ya. Yang, B. Duschatko, Y. Yuan, P. M. Ajayan, J. C. Idrobo, P. Narang and J. Miao, arXiv:1901.00633 (2019).

93. D. Ren, M. Chen, L. Waller and C. Ophus, arXiv:1807.03886 (2018).

Figure Captions

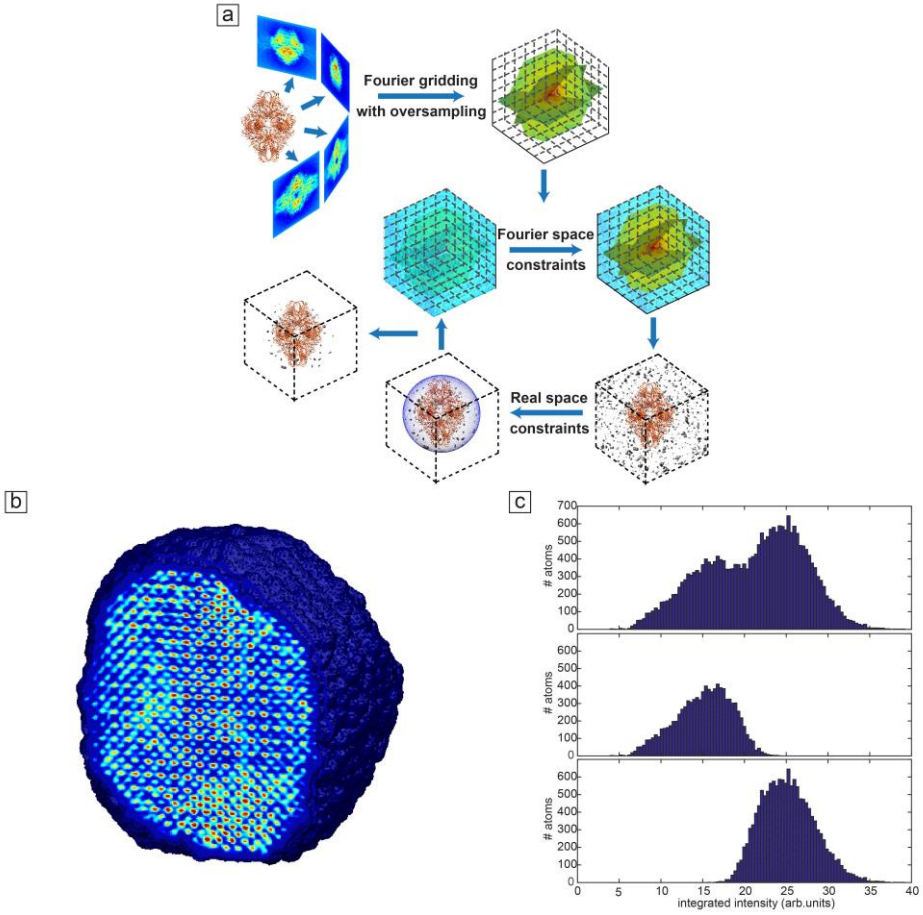

Figure 1. (a) An illustration of the GENFIRE algorithm. Adapted from Reference 75. © 2017, Springer Nature. (b) A cross-sectional view of a GENFIRE reconstruction volume from an FePt nanoparticle. Each local maxima represents the position of individual atoms, and Fe and Pt chemical species can be

distinguished from the intensity contrast. (c) Histogram of the identified local intensity peaks. An unbiased atom classification method was applied to separate these peaks, and classified 23,804 atom candidates into 9,588 Fe (middle panel) and 14,216 Pt (bottom panel) atom candidates. Adapted from Reference 55. © 2017, Springer Nature.

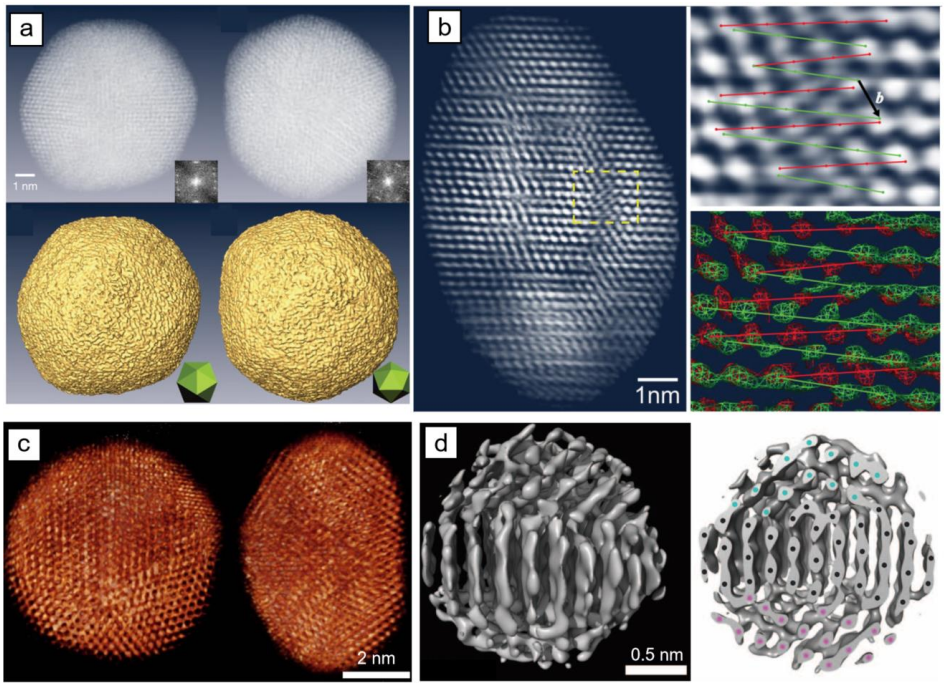

Figure 2. 3D atomic imaging of nanostructures using electron tomography. (a) 3D imaging of a gold nanoparticle at 2.4 Å resolution without assuming crystallinity or using averaging. Top shows the volume renderings of the 3D reconstruction of a gold nanoparticle and their Fourier transforms (insets) along the two- and threefold symmetry directions. Bottom shows the surface renderings of the 3D reconstruction with icosahedron model inset along the same symmetry directions. Adapted from Reference 41. © 2012, Springer Nature. (b) 3D imaging of dislocations in a platinum particle at atomic resolution. (left) 5.3 Å thick internal slice (two atomic layers) of the nanoparticle reconstructed by AET. (right) 3D volume and surface renderings of an enlarged view of the core of a screw dislocation with the Burgers vector (b) of 21 ½[011]. Adapted from Reference 54. © 2013, Springer Nature. (c) 3D reconstructions of a Ag-Au nanocluster. The volume-rendered 3D view shows atomic structure and composition of the cluster; Adapted from Reference 77. © 2015, Springer Nature. (d) Volume-rendered and cross-sectional views of the 3D structure of individual nanoparticle in liquid at near-atomic resolution. Adapted from Reference 78. © 2015, American Association for the Advancement of Science.

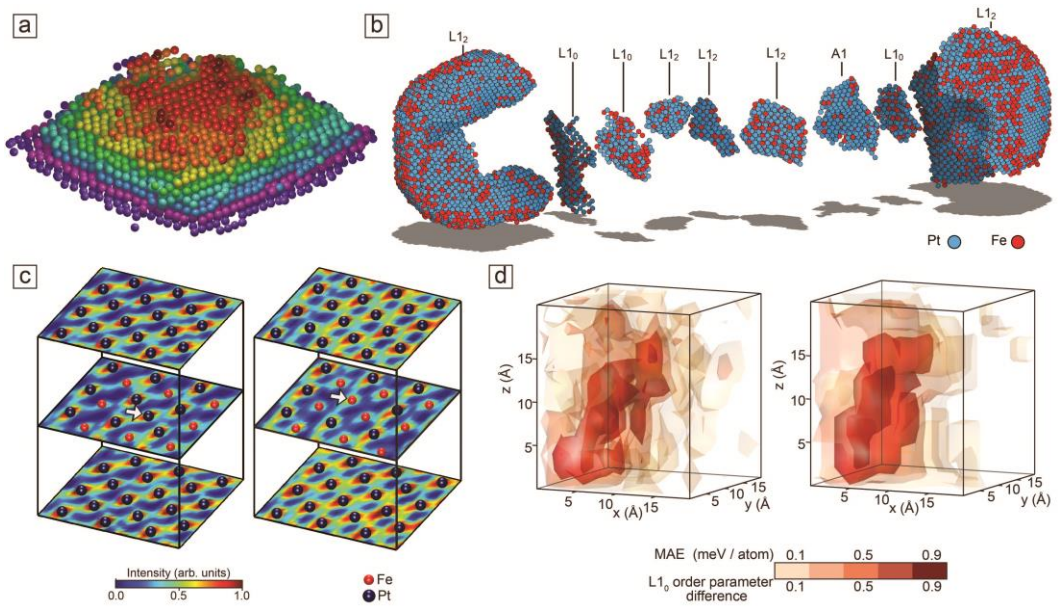

Figure 3. (a) Experimentally determined 3D positions of individual atoms in a tungsten needle sample revealed by electron tomography. The 3D atomic model of the sample consists of nine atomic layers along the [011] direction, labelled with dark red, red, orange, yellow, green, cyan, blue, magenta and purple from layers 1–9, respectively. Adapted from Reference 42. © 2015, Springer Nature. (b) Experimentally determined complex grain structure of an FePt nanoparticle via AET. The nanoparticle consists of two large $L1_2$ grains, three small $L1_2$ grains, three small $L1_0$ grains and a Pt-rich A1 grain. (c) 3D atomic positions overlaid on the 3D reconstructed intensity (color scale at bottom) illustrating anti-site point defects (arrows): a Pt atom occupying an Fe atom site (left), an Fe atom occupying a Pt atom site (right). (d) 3D iso-surface rendering of the calculated local MAE (left) and $L1_0$ order parameter differences (right) obtained from an $L1_0$ ordered grain within the nanoparticle. Adapted from Reference 55. © 2017, Springer Nature.

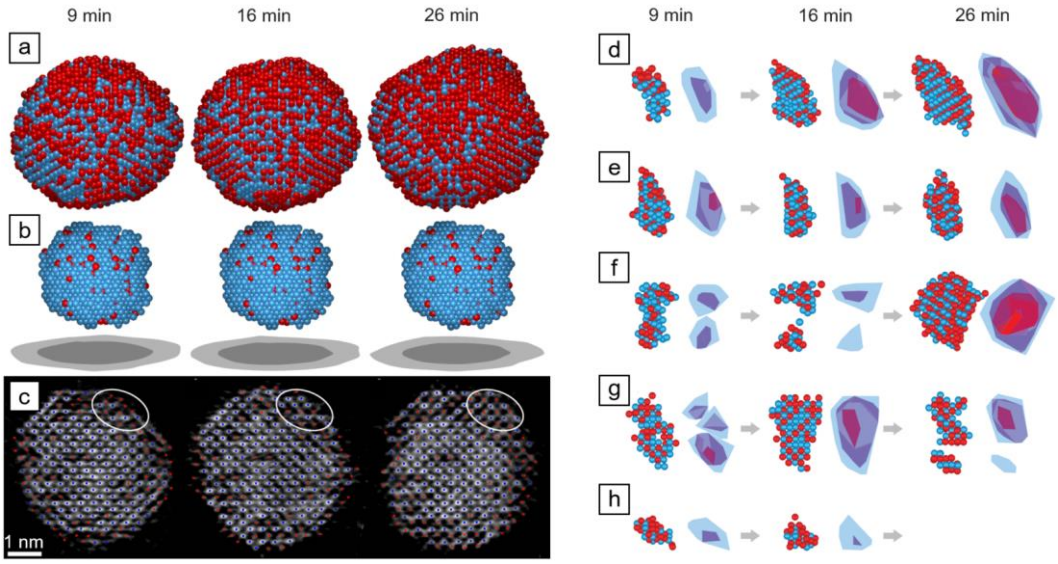

Figure 4. Capturing 4D atomic motion with AET. (a) 3D atomic models (Fe in red and Pt in blue) of an FePt nanoparticle with an accumulated annealing time of 9 min, 16 min and 26 min, respectively. (b) The Pt-rich core of the nanoparticle (shown here) remained the same for the three annealing times. The light and dark grey projections below the models show the whole nanoparticle and the core, respectively. (c) The same internal atomic layer of the nanoparticle along the [010] direction at the three annealing times, where a fraction of the surface and subsurface atoms had rearranged to form L10 phase (ellipses). (d-h), Representative growing (d), fluctuating (e-f), dissolving nuclei (g) with an accumulated annealing time of 9 min, 16 min and 26 min, respectively. The atomic models show Fe (red) and Pt (blue) atoms with an order parameter ≥0.3, and the 3D contour maps show the distribution of an order parameter of 0.7 (red), 0.5 (purple) and 0.3 (light blue). Adapted from Reference 56. © 2019, Springer Nature.

Author biographies

Jihan Zhou
Lawrence Berkeley National Laboratory
1 Cyclotron Rd. MS 72-150
Berkeley, CA 94720
Telephone: +1 510-486-6036
Email: jihan.zhou@physics.ucla.edu

Jihan Zhou is an assistant project scientist of Physics & Astronomy at UCLA. He received his bachelor's degree in chemistry and PhD degree in polymer chemistry and physics at Peking University in 2009 and 2014, respectively. He subsequently finished a postdoc position at UCLA, during which he performed the first 4D

AET experiment on capturing early stage nucleation. His research focuses on using and developing advanced electron microscopy and atomic electron tomography to solve traditionally intractable problems in chemistry, physics, materials science and nanoscience at atomic level.

Yongsoo Yang
Mailing address: Department of Physics, Korea Advanced Institute of Science and Technology (KAIST), Daejeon 34141, South Korea.
Telephone: +82 42 350 7303
Fax: +82 42 350 2510
Email: yongsoo.yang@kaist.ac.kr

Yongsoo Yang is an assistant professor at Department of Physics, Korea Advanced Institute of Science and Technology (KAIST). He received his bachelor's degree in physics and mathematical science from Seoul National University, and PhD degree in physics from the University of Michigan, followed by postdoctoral research at UCLA. His research focuses on structural determination beyond conventional crystallography, to resolve multi-dimensional (3D + time, temperature, external field, etc.) atomic structure of materials with surface/interface or defects where perfect crystal symmetry is broken.

Peter Ercius
Lawrence Berkeley National Laboratory
1 Cyclotron Rd. MS 72-150
Berkeley, CA 94720
Telephone: +1 510-486-4634
Email: percius@lbl.gov

Peter Ercius is a staff scientist at the National Center for Electron Microscopy (NCEM) facility within the Molecular Foundry Division at Lawrence Berkeley National Laboratory. He received his Bachelors of Science and PhD at Cornell University from the Applied and Engineering Physics Department in 2003 and 2009, respectively. He subsequently finished a postdoc position at the NCEM facility before being hired as a staff scientist which is his current position. His directs and oversees the electron tomography program at NCEM as well as being

the main staff contact for the TEAM 0.5 aberration corrected instrument. His research focuses on atomic resolution electron tomography, scanning nanodiffraction, *in situ* liquid cell electron microscopy and 2D/3D image analysis.

Jianwei (John) Miao
475 Portola Plaza,
Los Angeles, CA 90095-1547
Telephone: +1 310-206-2645
Email: miao@physics.ucla.edu

Jianwei (John) Miao is Professor of Physics & Astronomy at UCLA. In 1999, he performed the seminal experiment of extending X-ray crystallography to allow structural determination of non-crystalline specimens, which is known as coherent diffractive imaging (CDI), lensless or computational microscopy. CDI methods such as ptychography and Bragg CDI have been broadly implemented using synchrotron radiation, X-ray free electron lasers, high harmonic generation, optical lasers, and electrons. Another important field that Miao has pioneered is atomic electron tomography (AET). In 2012, he led a team that first demonstrated AET at 2.4 Å resolution without assuming crystallinity or averaging. He and collaborators have since performed several groundbreaking AET experiments and recently developed 4D AET to observe crystal nucleation at atomic resolution, showing early stage nucleation results not consistent with classical nucleation theory.